Available online at www.sciencedirect.com
SCIENCE DIRECT®
Journal of Solid State Chemistry 176 (2003) 567–574
JOURNAL OF SOLID STATE CHEMISTRY
http://elsevier.com/locate/jssc

The binary gallide Eu_5Ga_9 – crystal structure, chemical bonding and physical properties

Yuri Grin,[a,*] Walter Schnelle,[a] Raul Cardoso Gil,[a] Olga Sichevich,[a,b] Ralf Müllmann,[c] Bernd D. Mosel,[c] Gunter Kotzyba,[d] and Rainer Pöttgen[d,1]

[a] *Max-Planck-Institut für Chemische Physik fester Stoffe, Nöthnitzer Straße 40, 01187 Dresden, Germany*
[b] *Institute of Chemistry, Ukrainian State Forestry Academy, General Chuprynka Street 103, 290057 Lviv, Ukraine*
[c] *Institut für Physikalische Chemie, Universität Münster, Schlossplatz 4/7, 48149 Münster, Germany*
[d] *Institut für Anorganische und Analytische Chemie, Universität Münster, Wilhelm-Klemm-Straße 8, 48149 Münster, Germany*

Received 5 March 2003; received in revised form 23 May 2003; accepted 4 June 2003

Abstract

The title compound was prepared from the elements by reaction in a sealed tantalum tube at 1320 K followed by slow cooling to 970 K or, alternatively, in glassy carbon crucibles with HF melting. The crystal structure of Eu_5Ga_9 was refined from single-crystal data: *Cmcm*, $a = 4.613(1)$ Å, $b = 10.902(3)$ Å, $c = 26.097(6)$ Å, $Z = 4$, $R_F = 0.036$, 811 structure factors and 46 variables. The structure is described as a three-dimensional network formed by gallium atoms with europium atoms embedded in the cavities. The bonding analysis (LMTO, ELF) confirmed this representation of the structure. Magnetic susceptibility measurements show Curie–Weiss behavior above 60 K with a magnetic moment per Eu atom of $8.12(1)\,\mu_B$, indicating divalent europium. Eu_5Ga_9 orders antiferromagnetically at 19.0(5) K with re-ordering at 6.0(5) K. The electrical resistivity shows a metallic temperature dependence and magnetic scattering. ^{151}Eu Mössbauer spectroscopic experiments are compatible with divalent europium and show complex magnetic hyperfine field splitting below the ordering temperature.

Keywords: Europium; Gallide; Crystal structure; Magnetism; Chemical bonding; Mössbauer spectroscopy

1. Introduction

The binary system europium-gallium has been intensively investigated in the past [1–3]. Within this system six intermetallic compounds have been found and structurally characterized: Eu_3Ga_2 [4], EuGa [4], Eu_3Ga_5 [5], $EuGa_2$ [6–9], Eu_3Ga_8 [10,11] and $EuGa_4$ [2, 10, 12]. Nevertheless, there are still some discrepancies concerning e.g. the structure of europium digallide. An AlB_2-type [6,7] and a KHg_2-type structure [8,9] were reported. Later it was shown, that the AlB_2-derived structure is, in fact, formed in the high-temperature phase $Eu_{1-x}Ga_{2+3x}$ ($x \approx 0.05$) [13].

In the course of our systematic studies of binary and ternary intermetallic europium gallides [14,15] we were successful in preparing the new binary gallide Eu_5Ga_9, with a composition near to the digallide. Herein we give a full account on the structure refinement and a chemical bonding analysis of Eu_5Ga_9 and report on the magnetic, electrical, and ^{151}Eu Mössbauer spectroscopic studies.

2. Experimental

2.1. Synthesis

Starting materials for the preparation of Eu_5Ga_9 were ingots of europium (Johnson Matthey, stated purity 99.9%) and gallium lumps (ChemPur, stated purity 99.99%). Europium was redistilled before use. The large europium ingots were cut into smaller pieces and kept under argon prior to the reactions. Careful handling of the europium ingots was necessary in order to minimize impurities such as ferromagnetic EuO or EuN. The

*Corresponding author. Fax: 49-351-4646-4002.
E-mail addresses: grin@cpfs.mpg.de (Yu Grin), pottgen@uni-muenster.de (R. Pöttgen).
[1] Also for correspondence.

0022-4596/03/$ - see front matter © 2003 Elsevier Inc. All rights reserved.
doi:10.1016/S0022-4596(03)00332-3

argon was purified over molecular sieves and titanium sponge (900 K).

The elemental components were mixed in the 5:9 atomic ratio and sealed in a tantalum tube under an argon pressure of about 800 mbar. The tantalum tube was subsequently sealed in a silica tube to prevent oxidation and in a first step annealed at 1320 K for 2 days. The temperature was then lowered by 50 K every other day and finally held at 870 K for two weeks. This temperature (<1070 K for peritectic formation temperature, see Section 3) was chosen for annealing in order to obtain single-phase material in reasonable time. After switching off the heating and cooling in the closed furnace, the silvery product could easily be separated quantitatively from the tantalum tube. Alternatively, the elements were reacted in an open glassy carbon crucible under an argon atmosphere by high-frequency melting. Both synthetic routes lead to the single-phase samples (checked by X-ray powder diffraction and metallography).

2.2. DTA analysis

The thermal behavior of the prepared material was investigated with a DTA/TG system (STA 409C, Netzsch, heating rate 5 K/min) in Al_2O_3 crucibles under flowing argon (purified with Oxysorb).

2.3. X-ray investigations

A Guinier powder diffraction pattern of the sample was recorded with Cu$K\alpha_1$ radiation using α-quartz ($a=4.9130$ Å, $c=5.4046$ Å) as an internal standard. To assure correct indexing of the diffraction lines, the observed pattern was compared with the calculated one [16] using the positional parameters of the refined structure.

Single-crystal diffraction data were collected by use of the Stoe imaging plate diffraction system (IPDS) with graphite monochromatized Ag$K\alpha$ radiation. Crystallographic calculations were performed using the program package WinCSD [17]. All relevant information concerning the data collection and handling are listed in Table 1.

2.4. Magnetic susceptibility and electrical resistivity

Magnetization data for two polycrystalline samples were measured with different SQUID-magnetometers (MPMS 5 and XL7, Quantum Design) between 1.8 and 400 K in external fields up to 70 kOe ($B_{ext}=7$ T). The results were essentially identical and so only data for one sample are presented. The electrical resistance was determined on a rectangular block of polycrystalline material by a conventional dc four-probe method between 3.8 and 320 K. Any contact of the material with air was prevented when mounting the samples to the cryostats.

Table 1
Crystallographic data for Eu_5Ga_9

Empirical formula	Eu_5Ga_9
Formula weight	1387.33 g/mol
Wavelength	0.56087 Å
Crystal system	orthorhombic
Space group	*Cmcm* (No. 63)
Unit cell dimensions	$a=4.613(1)$ Å
(powder diffraction data)	$b=10.902(3)$ Å
	$c=26.097(6)$ Å
	$V=1312.4(9)$ Å^3
Formula units per cell	$Z=4$
Calculated density	7.02 g/cm^3
Crystal size	$0.07\times0.07\times0.19$ mm^3
Scan type	$\varphi, \Delta\varphi = 0.50$(phi)
Absorption correction	Analytical
Transmission ratio (max/min)	1.342/0.846
Absorption coefficient	22.35 mm^{-1}
2θ range for data collection	$5^\circ \leqslant 2\theta \leqslant 45^\circ$
hkl range	$-6\leqslant h\leqslant 6$, $-14\leqslant k\leqslant 13$, $-35\leqslant l\leqslant 33$
Total number of reflections	6522
Independent reflections	1013 ($R_{int}=0.05$)
Refinement method	Full-matrix least-squares on F
Data/parameters	811/46
Final R indices [$F>2\sigma(F)$]	$R_F=0.036$, $wR(F^2)=0.042$
R indices (all data)	$R_F=0.052$, $wR(F^2)=0.044$
Extinction coefficient	0.0023(1)

2.5. Mössbauer spectroscopy

^{151}Europium Mössbauer experiments were performed on a polycrystalline sample from the same batch as for the susceptibility measurements. The ^{151}Sm:EuF_3 source was held at room temperature while the temperature of the absorber was varied between 4.2 and 300 K.

2.6. Electronic structure calculations

For TB-LMTO calculations, the TB-LMTO-ASA program package [18] with exchange correlation potential according to Barth and Hedin [19] was used. The radial scalar-relativistic Dirac equation was solved to get the partial waves. The calculation within the atomic sphere approximation (ASA) includes corrections for ignoring of the interstitial regions and the partial waves of higher order [20]. In case of Eu_5Ga_9 the addition of empty spheres was not necessary. The following radii of atomic spheres were applied for calculations: r(Eu1) = 2.222 Å, r(Eu2) = 2.191 Å, r(Eu3) = 2.191 Å, r(Ga1) = 1.403 Å, r(Ga2) = 1.403 Å, r(Ga3) = 1.402 Å, r(Ga4) = 1.404 Å, r(Ga5) = 1.403 Å.

The electron localization function (ELF, η) was evaluated according to [21] within the TB-LMTO-ASA program package [18] with an ELF module already implemented. To get more insight to the chemical

Table 2
Atomic coordinates and anisotropic displacement parameters U_{ij} (Å^2) for Eu_5Ga_9. U_{eq} is defined as one-third of the trace of the orthogonalized U_{ij} tensor

Atom	Site	x	y	z	$U_{11}\cdot 10^2$	$U_{22}\cdot 10^2$	$U_{33}\cdot 10^2$	$U_{23}\cdot 10^2$	$U_{eq}\cdot 10^2$
Eu1	8*f*	1/2	0.15042(1)	0.45856(5)	0.90(7)	1.05(7)	1.02(7)	0.05(5)	0.99(4)
Eu2	8*f*	0	0.15647(1)	0.66728(6)	0.90(7)	1.01(7)	1.04(7)	0.14(5)	0.98(4)
Eu3	4*c*	0	0.1281(2)	1/4	1.2(1)	1.1(1)	1.0(1)	0	1.10(6)
Ga1	8*f*	1/2	0.0445(3)	0.33944(1)	1.0(2)	1.1(2)	1.1(1)	−0.2(1)	1.05(9)
Ga2	8*f*	0	0.0474(3)	0.54718(1)	0.8(2)	0.8(1)	1.3(1)	−0.1(1)	0.95(8)
Ga3	8*f*	0	0.1337(3)	0.37704(1)	0.9(2)	1.0(2)	1.2(2)	−0.3(1)	1.04(9)
Ga4	8*f*	1/2	0.1364(3)	0.58410(1)	0.8(2)	1.2(2)	0.9(1)	−0.1(1)	0.99(9)
Ga5	4*c*	1/2	0.0769(5)	3/4	1.3(2)	1.2(2)	0.7(2)	0	1.1(1)

The anisotropic displacement factor exponent takes the form $-2\pi^2[(ha^*)^2U_{11}+\cdots+2hka^*b^*U_{12}]$. $U_{12}=U_{13}=0$.

bonding, ELF was analyzed with the program Basin [22]. An integration of the valence electron density in the basins defined by surfaces of zero flux in ELF gradient gave, analogous to the procedure proposed by Bader for the electron density [23], the electron counts for each basin, which are important for the description of the bonding situation.

3. Results and discussion

Polycrystalline samples of Eu_5Ga_9 are light gray with metallic lustre and relatively stable in air. Single crystals have irregular platelet-like shape. Based on the DTA data, Eu_5Ga_9 forms peritectically at 1070(10) K.

The X-ray diffraction pattern could easily be indexed on the basis of the orthorhombic base-centered cell. The lattice parameters were obtained by a least-squares refinement of the Guinier powder data: $a=4.613(1)$ Å, $b=10.902(3)$ Å and $c=26.097(6)$ Å.

3.1. Crystal structure determination

Single crystals of Eu_5Ga_9 suitable for X-ray investigation were isolated from the sample by mechanical fragmentation and examined on a four-circle diffractometer as well as on the IPDS system. To be sure about the extinction conditions, also the primitive reflections were measured during the data collection, however, an analysis of the data set confirmed the *C* centered lattice. The starting atomic parameters were obtained from direct methods and the structure was successfully refined with anisotropic displacement parameters for all atoms. The residuals and atomic coordinates are listed in Tables 1 and 2; interatomic distances are given in Table 3.

In order to discuss the chemical bonding in Eu_5Ga_9 (see Section 3.5), we first investigated magnetic properties and Mössbauer effect to obtain information about the electronic state of europium as well as transport properties for more complete characterization of the title compound.

Table 3
Interatomic distances (Å) in the structure of Eu_5Ga_9

Eu1:	2	Ga3	3.143(3)		Ga1:	1	Ga5	2.683(4)	
	2	Ga2	3.161(3)			2	Ga3	2.689(3)	
	1	Ga4	3.280(4)			1	Ga4	2.806(5)	
	1	Ga2	3.298(4)			2	Eu2	3.186(3)	CN = 10
	1	Ga1	3.316(4)			1	Eu2	3.264(4)	
	1	Ga4	3.319(4)	CN = 18		1	Eu1	3.316(4)	
	2	Ga2	3.454(3)			2	Eu3	3.406(3)	
	2	Ga4	3.458(3)						
	2	Eu1	3.836(2)		Ga2:	1	Ga2	2.671(5)	
	1	Eu2	3.901(2)			2	Ga4	2.681(2)	
	1	Eu1	3.929(2)			1	Ga3	2.794(5)	
	2	Eu1	4.613(1)			2	Eu1	3.161(3)	CN = 10
						1	Eu1	3.298(4)	
Eu2:	2	Ga4	3.175(3)			1	Eu2	3.352(4)	
	2	Ga1	3.186(3)			2	Eu1	3.454(3)	
	1	Ga1	3.264(4)						
	2	Ga5	3.276(2)		Ga3:	2	Ga1	2.689(3)	
	1	Ga2	3.352(4)			1	Ga4	2.703(5)	
	1	Ga3	3.368(4)			1	Ga2	2.794(5)	
	2	Ga3	3.448(3)	CN = 18		2	Eu1	3.143(3)	CN = 10
	1	Eu3	3.780(2)			1	Eu3	3.316(3)	
	1	Eu1	3.901(2)			1	Eu2	3.368(4)	
	2	Eu3	3.937(2)			2	Eu2	3.448(3)	
	1	Eu3	4.318(2)						
	2	Eu2	4.613(1)						
					Ga4:	2	Ga2	2.681(2)	
						1	Ga3	2.703(5)	
Eu3:	2	Ga5	3.212(4)			1	Ga1	2.806(5)	
	1	Ga5	3.216(5)			2	Eu2	3.175(3)	CN = 10
	2	Ga3	3.316(3)			1	Eu1	3.280(4)	
	4	Ga1	3.406(3)	CN = 17		1	Eu1	3.319(4)	
	2	Eu2	3.780(2)			2	Eu1	3.458(3)	
	4	Eu2	3.937(2)						
	2	Eu3	4.613(1)		Ga5:	2	Ga1	2.683(4)	
						2	Eu3	3.212(4)	CN = 9
						1	Eu3	3.216(5)	
						4	Eu2	3.276(2)	

All distances shorter than 5.20 Å (Eu–Eu), 4.85 Å (Eu–Ga) and 3.85 Å (Ga–Ga) are listed.

3.2. Magnetic properties

The temperature dependence of the inverse magnetic susceptibility $1/\chi(T)$ of Eu_5Ga_9 in a field of 10 kOe

($B_{ext} = 1$ T) is presented in Fig. 1. Eu_5Ga_9 shows Curie–Weiss behavior above 60 K with an effective magnetic moment μ_{eff}/Eu-atom $= 8.12(1)\,\mu_B$ and a quite small Weiss temperature $\Theta = +1.3(1)$ K obtained from a fit of $\chi(T) = C/(T-\Theta)$ to experimental data in the range of 60 K $< T <$ 400 K). μ_{eff} is in agreement with that of all europium atoms in the $^8S_{7/2}$ groundstate of the $4f^7$ configuration (Eu^{+2}; $\mu_{free} = 7.94\,\mu_B$). A small enhancement of μ_{eff} is due to the presence of conduction electrons. Only for fields as small as $H_{ext} = 100$ Oe a barely visible anomaly in $\chi(T)$ at $\approx$70 K hints for the presence of traces of strongly ferromagnetic EuO ($T_C = 69$ K). The low-temperature behavior of $\chi(T, 10\,\text{kOe})$ is given in the inset of Fig. 1. Two cusps are visible at $T_{N1} = 19.0(5)$ K and $T_{N2} = 6.0(5)$ K. The anomalies can be assigned to the antiferromagnetic ordering of the $4f^7$ moments of Eu species from different crystallographic sites of the structure. An assignment of the ordering temperatures T_{N1} and T_{N2} to the three crystallographic different sites is not possible without e.g. specific heat capacity or spin structure data.

Isothermal magnetization data for both increasing (up to 70 kOe) and decreasing field were recorded at different temperatures in the ordered phases and in the paramagnetic phase of Eu_5Ga_9 (Fig. 2). For $T = 40$ K the isotherm is slightly curved and follows the Brillouin function for $J = 7/2$ paramagnetic moments, however, for $T = 20$ K the isotherm $M(H)$ already falls below the Brillouin curve. The initial ($H < 30$ kOe) slope of $M(H)$ is the same for all isotherms with $T \leqslant 20$ K, but for the curves at $T \leqslant 10$ K a change of curvature at 30(3) kOe indicates the onset of a metamagnetic transition. This transition is seen more clearly in $M(1.8\,\text{K})/H$ which is plotted in the inset of Fig. 2. The metamagnetic transition is broad, has only a small field hysteresis and continues up to 46(4) kOe. The magnetic moment shows no tendency towards saturation and reaches a value of 4.1 μ_B per Eu-atom for the point with the largest ratio H/T (70 kOe at 1.8 K), much less than the expected saturation moment of 7.0 μ_B for divalent europium. In view of the three crystallographic different Eu positions the magnetic phase diagram of Eu_5Ga_9 is expected to be complex and scarcely illuminated by these first experiments.

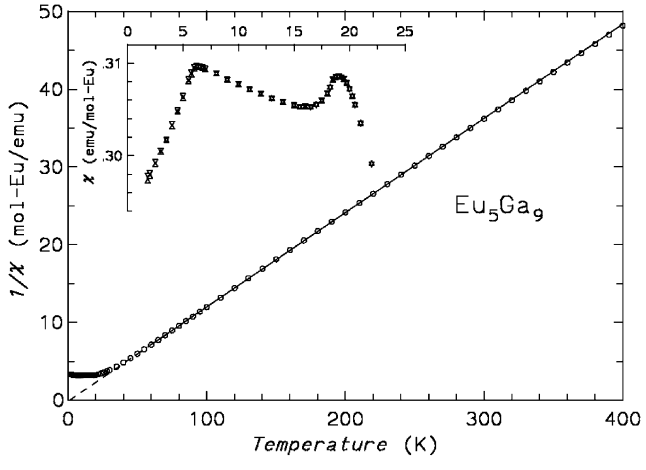

Fig. 1. Temperature dependence of the inverse magnetic susceptibility $1/\chi(T)$ of Eu_5Ga_9 as measured in a magnetic field of 10 kOe ($B_{ext} = 1$ T). The low-temperature behavior of $\chi(T)$ is shown in the inset. Up and down triangles stand for the zero-field cooled measurement taken during warming and field cooling measurements, respectively.

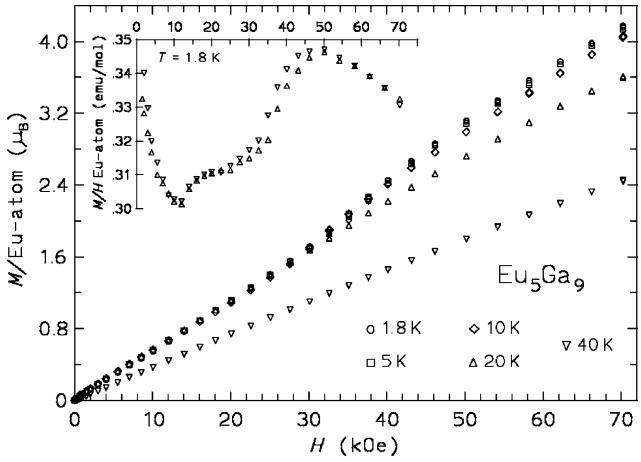

Fig. 2. Magnetic moment vs (?) external magnetic field $M(H)$ for Eu_5Ga_9 at different temperatures. The inset shows M/H for $T = 1.8$ K where up and down triangles indicate increasing or decreasing field.

3.3. Mössbauer spectroscopy

The ^{151}Eu Mössbauer spectra of Eu_5Ga_9 at 78, 20 and 4.2 K are shown in Fig. 3 together with the transmission integral fits. The fitting parameters for these and some additional measurements are listed in Table 4. Above the antiferromagnetic ordering temperature of 25(1) K (as determined by ^{151}Eu Mössbauer spectroscopy) a single line is detected in the Eu^{II} region with an isomer shift $\delta = -10.2$ mm/s at 78 K. In the Eu^{III} region an impurity component of about 3% can be seen at $\delta = 1.0$ mm/s at 78 K which is included as a simple Lorentzian in all fits but not reported in the table. The increased line width (normally such an europium intermetallic compound shows a line width of about 2.3 mm/s) is due to the superposition of the very similar lines of the three crystallographically different europium sites. Within the temperature range 15 K $< T <$ 25 K, the Eu^{II} spectrum can be described as a superposition of a magnetically ordered component and a non-split one. The fraction of the latter decreases with temperature, an effect which might be due to a volume distribution of the magnetic particle sizes or to a stepwise ordering of the three different europium positions. With decreasing temperature the magnetic hyperfine field increases and

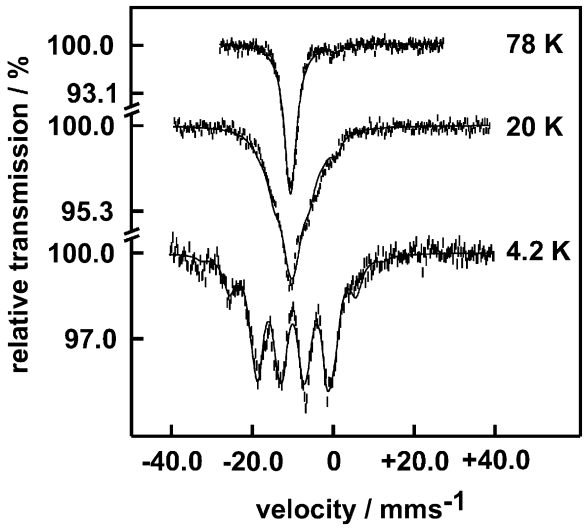

Fig. 3. Experimental and simulated ^{151}Eu Mössbauer spectra of Eu_5Ga_9.

Table 4
Fitting parameters of ^{151}Eu Mössbauer measurements in Eu_5Ga_9

T (K)	δ (mm/s)	Γ (mm/s)	$\lvert B\rvert$ (T)	X_{mag}
78.0	−10.2(1)	3.1(2)	—	—
27.0	−9.8(1)	3.1(2)	—	—
26.0	−9.9(1)	3.1	—	—
25.0	−9.9(1)	3.2(2)	1.4(6)	0.39
20.0	−9.8(1)	4.1(8)	10.7(8)	0.74
15.0	−9.5(1)	3.0	17.3(3)	0.97
10.0	−9.7(2)	2.9(5)	20.2(6)	1
4.2	−9.6(1)	3.0(3)	21.6(3)	1

Numbers in parentheses represent the statistical errors in the last digit. Parameters without parentheses were kept fixed. X_{mag} indicates the fraction of magnetically split europium atoms.

amounts to $B_{sat} = 21.6(3)$ T at 4.2 K. Such high hyperfine fields are typically observed for similar intermetallic compounds of europium [24].

3.4. Electrical resistivity

The electrical resistivity $\rho(T)$ of Eu_5Ga_9 is depicted in Fig. 4. $\rho(T)$ is linear for $T > 60$ K and the value $\rho(300\,\text{K})$ of $\approx 70\,\mu\Omega\,\text{cm}$ is of the order often found for structurally more complex intermetallic compounds. The magnetic phase transition temperatures cannot be located in $\rho(T)$. Instead, a broad hump at temperatures below 60 K and a moderate decrease of $\rho(T)$ is seen. From the large deGennes factor for the $4f^7$ configuration of Eu a more pronounced effect could be expected at the antiferromagnetic ordering. The width of the hump in $\rho(T)$ might be due to the complex magnetic structure of Eu_5Ga_9.

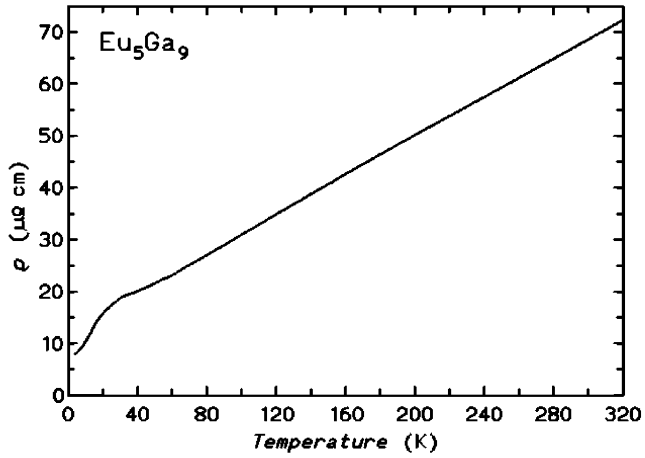

Fig. 4. Electrical resistivity vs (?) temperature $\rho(T)$ of polycrystalline Eu_5Ga_9.

3.5. Crystal structure and chemical bonding

From the crystallographic information (Section 3.1), the Ga–Ga distances in the Eu_5Ga_9 structure vary in a narrow range between 2.68 and 2.80 Å (Table 3). Most gallium atoms (Ga1–Ga4) have four nearest gallium neighbors. Despite the similar interatomic distances, the tetrahedral environment of four-bonded (4b) atoms is somewhat distorted: the bond angles vary between 89.7° and 119.7°. Only Ga5 is two-bonded (2b) with the bond angle of 120.9°. The four- and two-bonded gallium atoms form a three-dimensional network (Fig. 5a). The europium atoms are located in the large cavities of this network. The coordination numbers of the europium atoms are practically equal (17 or 18, Table 3).

According to the Zintl concept the gallium part of the Eu_5Ga_9 structure can be written as $[(4b)Ga^{1-}]_8[(2b)Ga^{3-}]_1$. This requires $[Eu^{2+}]_4[Eu^{3+}]_1$ as counterpart and suggests the presence of trivalent europium in the structure. But both, magnetic susceptibility measurements and ^{151}Eu Mössbauer spectra, clearly show the absence of europium in the $4f^6$ configuration. Thus, according to $[Eu^{2+}]_5$, a maximum of ten electrons is transferred to the gallium network and one electron is missing per formula unit to satisfy the Zintl count.

In order to get a deeper understanding of the bonding situation in Eu_5Ga_9, the (total) electron localization function (ELF, η) was analyzed in detail. The positions of the ELF-attractors around the two-bonded Ga5 atoms are as expected. Two lone pair-like attractors and two attractors near to the Ga5–Ga1 contacts are observed. For the four-bonded Ga1 atoms all four respective attractors can be recognized (Fig. 6a). Similar situations are obtained for the four-bonded Ga2, Ga3 (Fig. 6b) and Ga4 atoms (Figs. 6a and b). In comparison with Ga1, we observe two attractors symmetrically

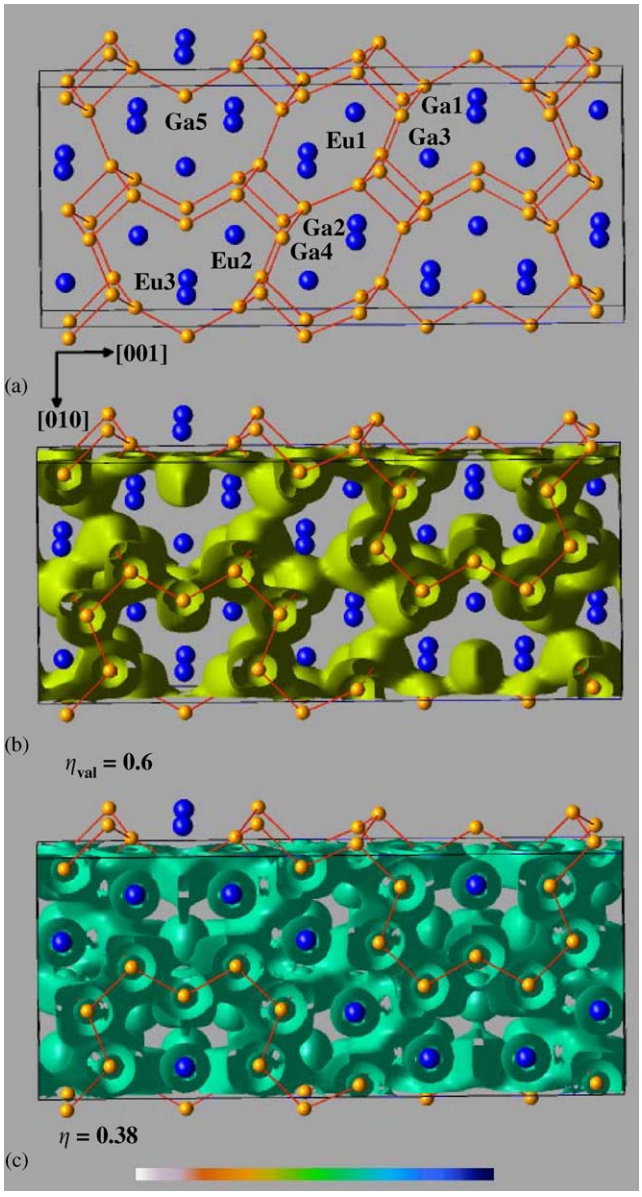

Fig. 5. The structure of Eu_5Ga_9: (a) three-dimensional gallium network with europium atoms in the cavities. (b) $\eta_{val} = 0.6$ localization domain for the gallium network (valence ELF). (c) $\eta_{val} = 0.38$ localization domain of the (total) ELF for the gallium network (for details see text).

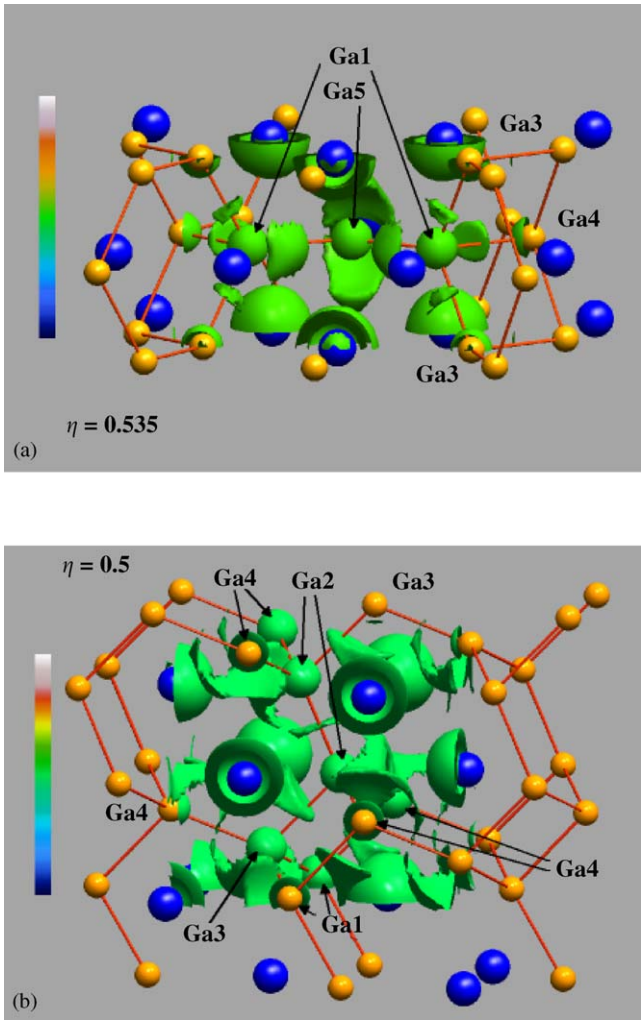

Fig. 6. Isosurface $\eta = 0.535$ of the (total) ELF in the surrounding of the Ga5 atoms; (b) isosurface $\eta = 0.5$ of the (total) ELF in the surrounding of Ga2 atoms (for details see text).

positioned around the bonds Ga2–Ga2 and Ga3–Ga4, respectively (Fig. 6b).

An integration of the valence electron density in the basins defined by zero-flux surfaces in the ELF gradient leads to the electron counts, which represent the lower limit for these values [25]. Nevertheless, integration resulted in counts of 1.7–2.1 electrons for the basins of the basin sets of four-bonded atoms, which would lead to roughly four electrons per gallium atom (i.e. Ga^{1-}). Only for the Ga5 environment, smaller counts were obtained: 1.8 electrons for the basin of the lone pair-like attractor and 1.4 electrons for basins of the Ga1–Ga5 bonds. This results in 5 electrons per Ga5 atom (i.e. Ga^{2-}) instead of the expected value of 6 for a Ga^{3-} situation.

All the basins of the above-mentioned attractors form valence shell basin sets [26] around the gallium atoms. The valence shell basin set of the whole network can be finally defined. The lowest interconnection points (ic) [26] in the network basin sets are observed at $\eta_{val,ic} = 0.65$ and $\eta_{ic} = 0.44$. This is illustrated with the localization domains [26] for $\eta_{val} = 0.6$ (Fig. 5b) and $\eta = 0.38$ (Fig. 5c), which are solely contained inside the respective network basin set. Integration of the valence electron density for the latter case gives a count of 140 electrons for the whole network within the unit cell instead of the expected count of 148 assuming all europium atoms in the $4f^7$ configuration. Thus, each europium atom has 7.4 electrons, while 7 electrons are expected. Taking the size of the unit cell into account, the deviation of about 6% from the expected value is acceptable.

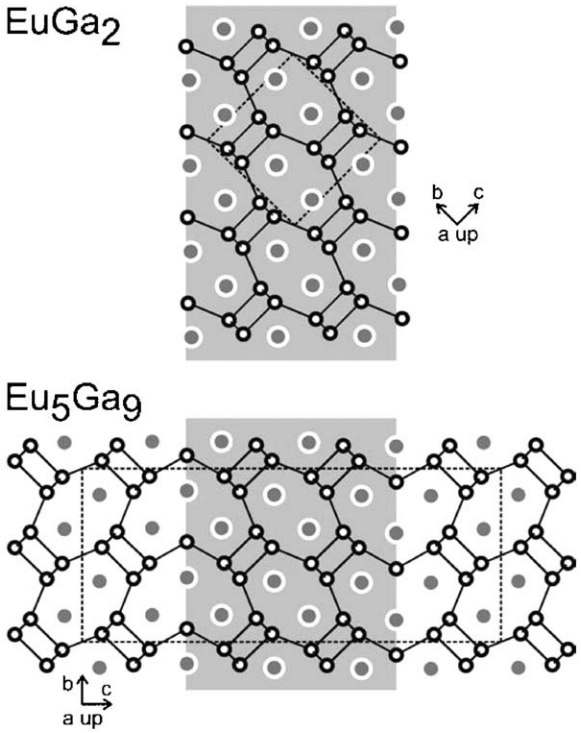

Fig. 7. Projection of the crystal structures of $EuGa_2$ (KHg_2 type, space group *Imma*) and Eu_5Ga_9 (space group *Cmcm*) onto the *yz* planes. The shaded slabs are similar in both structures (for details see text).

Practically equal electron counts for the three crystallographically different europium atoms correlate well with the very similar partial contributions of the *f* electrons to the density of states as obtained from the band structure calculation.

Summing up, from the analysis of the electron localization function in real space, the bonding situation in Eu_5Ga_9 can be written as $[Eu^{2+}]_5[Ga^{1-}]_8[Ga^{2-}]_1$ with divalent europium only. This correlates well with the results of magnetization measurements and ^{151}Eu Mössbauer spectroscopic experiments.

Finally, it is interesting to compare the Eu_5Ga_9 structure with the KHg_2 type structure of the digallide $EuGa_2$ [9,13]. As emphasized in Fig. 7, both structures have the same structural slab (shaded areas in Fig. 7). The Eu_5Ga_9 structure is build up from $EuGa_2$ related slabs by 'chemical twinning' (for the term see [27–31]). The $EuGa_2$ related slabs are *glued* together in Eu_5Ga_9 at the mirror planes at $z = 1/4$ and 3/4, respectively. The chemical twinning in Eu_5Ga_9 accounts for the different bonding situation in both gallides. The four-bonded gallium atoms in $EuGa_2$ build a three-dimensional network of corner-sharing $GaGa_4$ tetrahedra. Considering the divalent europium, a Zintl–Klemm formulation $[Eu^{2+}][Ga^{1-}]_2$ is adequate [13]. The chemical twinning in Eu_5Ga_9 leaves two-bonded gallium atoms on the mirror planes, and also the coordination number of the Eu3 atoms differs slightly from those of Eu1 and Eu2. The various Eu–Ga distances in both structures, however, cover almost the same range. A similar mechanism of chemical twinning has recently been observed for the closely related structures of $GdNiIn_2$ and $CeNiIn_2$ [32].

Acknowledgments

This work was supported by the Deutsche Forschungsgemeinschaft (Po573/1–4) and the Fonds der Chemischen Industrie. We thank D. Jerebtsov and R. Niewa for the DTA experiments as well as M. Kohout and F.R. Wagner for valuable discussions concerning bonding analysis in real space.

References

[1] S.P. Yatsenko, J. Chimie Physique 74 (1977) 836.
[2] S.P. Yatsenko, B.G. Semenov, K.A. Chuntonov, Russ. Metallurgy (1978) 173.
[3] S.P. Yatsenko, A.A. Semyannikov, B.G. Semenov, K.A. Chuntonov, J. Less-Common Met. 64 (1979) 185.
[4] M.L. Fornasini, S. Cirafici, Z. Kristallogr. 190 (1990) 295.
[5] Ju.N. Grin, S.P. Yatsenko, E.G. Fedorowa, N.A. Sabirsijanow, O.M. Sitschewitsch, Ya.P. Yarmolyuk, J. Less-Common Met. 136 (1987) 55.
[6] A. Iandelli, Z. Anorg. Allg. Chem. 330 (1964) 221.
[7] D.I. Dzyana, V.Y. Markiv, E.I. Gladyshevsky, Dopov. Akad. Nauk Ukr. RSR (1964) 1177.
[8] V.Ja. Markiv, N.N. Beljavina, T.I. Zhunkovska, Dopov. Akad. Nauk Ukr. RSR, Ser. A: Fiziko-Matematichni ta Tekhnichni Nauki 44 (1982) 84.
[9] K.H.J. Buschow, D.B. de Mooij, J. Less-Common Met. 97 (1984) L5.
[10] D.B. de Mooij, K.H.J. Buschow, J. Less-Common Met. 109 (1985) 117.
[11] S.P. Jacenko, O.M. Sichevich, Ja.P. Jarmoljuk, Ju.N. Grin, Dopov. Akad. Nauk Ukr. RSR, Ser. B: Geologichni, Khimichni ta Biologichni Nauki (1985) 55.
[12] P.I. Kripyakevich, E.I. Gladyshevskii, D.I. Dzyana, Sov. Phys. Crystallogr. 10 (1965) 392.
[13] O. Sichevich, R. Ramlau, R. Giedigkeit, M. Schmidt, R. Niewa, Yu. Grin, in: 13th International Conference on Solid State Compounds of Transition Metals, Stresa, Italy, 2000, p. O-13.
[14] R. Pöttgen, Y. Grin, Z. Kristallogr. 11 (Suppl.) (1996) 93.
[15] R. Pöttgen, Y. Grin, Z. Kristallogr. 12 (Suppl.) (1997) 137.
[16] K. Yvon, W. Jeitscho, E. Parthé, J. Appl. Crystallogr. 10 (1977) 73.
[17] L.G. Akselrud, P.Yu. Zavalii, Yu. Grin, V.K. Pecharsky, B. Baumgartner, E. Wölfel, Mater. Sci. Forum 335 (1993) 133.
[18] O. Jepsen, A. Burkhardt, O.K. Andersen, The Program TB-LMTO-ASA, Version 4.7. Max-Planck-Institut für Festkörperforschung, Stuttgart, 1999.
[19] U. Barth, L. Hedin. J. Phys. C 5 (1972) 1629.
[20] O.K. Andersen, Z. Pawlowska, O. Jepsen, Phys. Rev. B 34 (1986) 5253.
[21] A. Savin, H.J. Flad, J. Flad, H. Preuss, H.G. von Schnering, Angew. Chem. 104 (1992) 185;
A. Savin, H.J. Flad, J. Flad, H. Preuss, H.G. von Schnering, Angew. Chem. Int. Ed. Engl. 31 (1992) 185.
[22] M. Kohout, Basin, Version 2.3. Max-Planck-Institut für Chemische Physik fester Stoffe, Dresden, 2001.

[23] R.F.W. Bader, Atoms in Molecules: A Quantum Theory, Oxford University Press, Oxford, 1999.
[24] R. Pöttgen, D. Johrendt, Chem. Mater. 12 (2000) 875.
[25] M. Kohout, A. Savin. Int. J. Quantum Chem. 60 (1996) 875.
[26] M. Kohout, F.R. Wagner, Yu. Grin, Theor. Chem. Acc. 108 (2002) 150.
[27] E. Parthé, B. Chabot, in: K.A. Gschneidner Jr., L. Eyring (Eds.), Handbook on the Physics and Chemistry of Rare Earths, Vol. 6, North-Holland, Amsterdam, 1984, p. 113.
[28] K. Cenzual, E. Parthé, Acta Crystallogr. C 40 (1984) 1127.
[29] E. Parthé, B. Chabot, K. Cenzual, Chimia 39 (1985) 164.
[30] E. Parthé, Elements of Inorganic Structural Chemistry, Pöge, Leipzig (1990).
[31] S. Andersson, Angew. Chem. 95 (1983) 67.
[32] V.I. Zaremba, Ya.M. Kalychak, Yu.B. Tyvanchuk, R.-D. Hoffmann, M.H. Möller, R. Pöttgen, Z. Naturforsch. 57b (2002) 791.